



Characterization and properties of silicon carbide fibers with self-standing membrane structure



Xinmei Hou ^{a,*}, Enhui Wang ^a, Zhi Fang ^a, Junhong Chen ^b, Kuo-Chin Chou ^a

^a State Key Laboratory of Advanced Metallurgy, Collaborative Innovation Center of Steel Technology, University of Science and Technology Beijing, Beijing 100083, China

^b School of Material Science and Engineering, University of Science and Technology Beijing, Beijing 100083, China

ARTICLE INFO

Article history:

Received 30 May 2015

Received in revised form

14 July 2015

Accepted 16 July 2015

Available online 17 July 2015

Keywords:

SiC fiber

Microstructure

Membrane

Properties

ABSTRACT

SiC fibers with self-standing membrane structure in large scale are prepared by one-step thermal reduction method by using carbon black and gangue as raw material at 1500 °C for 2 h in argon. The average pore size of the membrane is 1.603 μm using the bubble-point method. The synthesized SiC fibers are well-developed cubic structure with the diameter in the range of 100–500 nm and length up to several millimeters. In addition, SiC fibers possess good oxidation resistance up to 1250 °C in air and low thermal expansion coefficient of $4.385\text{--}4.655 \times 10^{-6}/^{\circ}\text{C}$ from room temperature to 750 °C. The oxidation behavior of SiC fibers depends on temperature and sample shape. Based on this, the oxidation kinetics is dealt with the real physical picture (RPP) model and gets a good agreement with the experimental data.

© 2015 Published by Elsevier B.V.

1. Introduction

Ceramic fibers as a kind of fibrous lightweight material have drawn a significant amount of attention because of its excellent physical and chemical properties [1]. Among them, silicon carbide (SiC) fiber is characterized by high strength, corrosion resistance, good refractory and low density etc. [2,3]. Therefore it is extensively applied in the fields of diesel engines, aerospace, thermal conductor and fusion reactors etc. [3–10] as the key component in reinforced ceramic matrix composites (CMCs) under harsh working conditions. Considering its enormous potential application, much effort has been spent on synthesis and characterization of SiC fibers over the past decades. As for the fabrication techniques, various methods including chemical vapor phase growth deposition (CVD) [11–13], electron beam irradiation curing (EBIC) [14–16], electrospinning (ES) [17], polymer impregnation pyrolysis (PIP) [18–22], catalyst-assisted pyrolysis of polysilazane precursor (CAP) [23–30] and silicon gel carbon thermal reduction (SGCTR) [31,32] etc. have been reported and got some success in industrial production. However the methods of CVD and EBIC require strict condition and thus are at high costs. ES, PIP and PSN methods are characterized

with complex process and superior cost because they are prepared from specific precursors. Besides, SGCTR method is difficult to obtain uniform morphology. Therefore it's desirable to propose a new method to prepare SiC fibers efficiently and economically.

As for the properties of SiC fibers especially at high temperature, Takeda et al. [20] investigated the oxidation behavior of polycarbosilane-derived SiC fibers at 1000–1400 °C in air for 1–100 h. The result showed that the fibrous structure maintained well except that some pores and fractures appeared. Bunsell et al. [33] pointed out that there still much work remained to be done to keep the fiber stable above 1000 °C. Besides these, there is no further work to be carried out on the high temperature properties of SiC fibers. This brings a lot of difficulty for the application of materials, for instance, CMCs reinforced by SiC fibers.

Herein one-step carbon thermal reduction method was adopted to synthesize SiC fibers with uniform morphology using the raw materials of carbon black and the gangue. By controlling the atmosphere and temperature, large amount of SiC fibers with self-standing membrane structure was prepared. Considering the application of SiC fibers under harsh conditions, the high temperature properties of SiC fibers including the oxidation behavior up to 1450 °C in air and the thermal expansion coefficient from room temperature to 750 °C were also investigated.

Compared with SiC nanofibers/nanowires by using the thermal reduction of SiO₂ and active carbon reported in the

* Corresponding author.

E-mail address: houxinmei@ustb.edu.cn (X. Hou).

literature [34–40], the difference and advantage of our work are following: (1) In view of the synthesis condition, the reaction temperature and the ratio of gangue and carbon black are selected at a reasonable range in this work. This can avoid both the removal of the residual carbon [34,35] and too high reaction temperature [36]. (2) As for SiC fibers produced in this work, the synthesized SiC fibers are well-developed cubic structure with high purity and uniform morphology. The stacking defect (SF) of SiC fibers is relatively less than the reported result in the literature [37–40]. What's more, the synthesized product is self-assembled into membrane structure, showing its potential application as filter. (3) As for the properties of SiC fibers, less work about the thermal property of SiC fibers is reported. In this work, the properties of SiC fibers including oxidation resistance and thermal stability are investigated. These fundamental data may pave the way for the application of SiC fibers at high temperature.

2. Material and methods

2.1. Material preparation

Gangue ($\text{SiO}_2 > 99\%$) and carbon black were used as silicon and carbon sources respectively. The powder with the mole ratio of 1:3 (SiO_2/C) was ball mixed. Preparation of SiC fibers was mainly taken place in a high temperature furnace using carbon as the inner lining, which is described in detail in our recent work [41]. During the whole process, argon with the purity of 99.9% at the rate of 0.4 L/min was adopted as protecting atmosphere and the total pressure was kept at 0.1 MPa. When the furnace was cooled naturally to room temperature, argon was stopped and gray–white self-standing membrane in large scale was obtained mainly on the top of the furnace. The resulting fibers were washed with 10% hydrofluoric acid (HF) for 1 h to remove the remained silica.

2.2. Phase and microstructure characterization

The phase was characterized using a 21 kW extra-power powder X-ray diffractometer (XRD) (M21XVHF22, Mac Science Co. Ltd., Yokohama, Japan) with Cu $K\alpha$ ($\lambda = 1.54056 \text{ \AA}$) radiation over a 2θ range from 10 to 90° . The morphology and microstructure of the synthesized fibers were observed using a scanning electron microscopy (SEM: Model JSM-840A, JEOL, Tokyo, Japan) and transmission electron microscopy with SAED (TEM: Model Tecnai G2 F30 S-TWIN, FEI, America). The pore size of the fibrous membrane was investigated by a capillary flow porometer (IB-FT Germany, POROLUX 1000) based on bubble-point method [42,43].

2.3. High properties of SiC fibers

The thermal expansion coefficient of SiC fibers was determined using an advanced analyzer (SETARAM Setsys Evo TMA). The experiments were carried out in an accurate dilatometric cycle running measurements at the heating rate of $10^\circ\text{C}/\text{min}$ from room temperature to 750°C and then cooled to room temperature as a cycle at nitrogen atmosphere. In the experiment, the sample was pressed into the cylinder with 10 mm in diameter and 3 mm in height. The linear thermal expansion coefficient was calculated from the following equation:

$$\rho = \frac{L_T - L_0 + Ak(T)}{L_0} \quad (1)$$

where ρ is the linear thermal expansion coefficient ($1/^\circ\text{C}$). L_0 (mm) and L_T (mm) are the length of the sample at room temperature and

the experimental temperature T , respectively. $Ak(T)$ (mm) is the correction value of the instrument at the experimental temperature T .

The oxidation behavior of SiC fibers was investigated under both non-isothermal and isothermal conditions using a thermoanalyzer (Netzsch STA 449C, Netzsch, Germany). The TG microbalance had the sensitivity of 1 mg. Before isothermal oxidation experiments, non-isothermal oxidation from 600 to 1500°C at the heating rate of $10^\circ\text{C}/\text{min}$ in air was investigated to have knowledge of the oxidation behavior of SiC fibrous membrane. In the isothermal experiments, SiC fibers (about 7.1 mg) were placed in an alumina crucible and the temperature was rapidly raised to the required level in a flowing purified argon gas. After the thermal equilibrium was established, argon was stopped and air was then introduced. The mass change due to oxidation was then monitored continuously for 2 h at the rate of 2 point/min. In all the experiments, the flow rate of air was kept constant, i.e. 40 ml/min. To ensure the data to be as accurate as possible, every experiment was repeated at least three times and got the average value.

3. Results and discussion

3.1. Phase and microstructure characterization

Fig. 1 is the optical image of the synthesized product. It can be seen that it is self-assembled into membrane structure. The cross section of the membrane is consisted of SiC fibers as shown in the inset of Fig. 1. The XRD pattern as shown in Fig. 2 is indexed from left to right as (111), (200), (220) and (311) corresponding to 3C–SiC (Card No.104 01-073-1665), indicating that SiC with high purity is obtained. Traditionally, SF are frequently found in 3C–SiC [44], whose density can be measured by SF peak (about 33.6°) be divided by (200) peak (41.4°). In this work the SF peak almost disappeared and (200) peak was also very weak, indicating that the density of SF in the synthesized SiC fibers was relatively less.

Fig. 3a and b shows SEM images of the overall look of SiC at low magnification. It can be seen SiC fibers are uniform. At high magnification (Fig. 3c), SiC fibers are long and straight filaments with diameter between 100 and 500 nm and length up to several millimeters. In addition, the straight fibers possess a smooth surface. There are also some SiC fibers with the bamboo-like morphology (Fig. 3d). A large number of SEM examinations have been carried out. The bamboo-like whiskers account for 5% or so of the total fibers using statistical method.

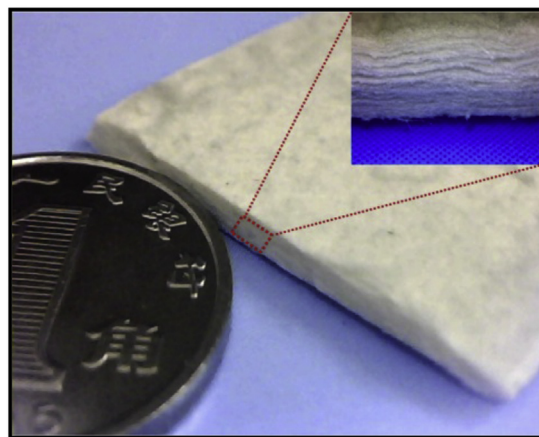


Fig. 1. Optical image of the synthesized SiC fibers and the inset of cross section at high magnification.

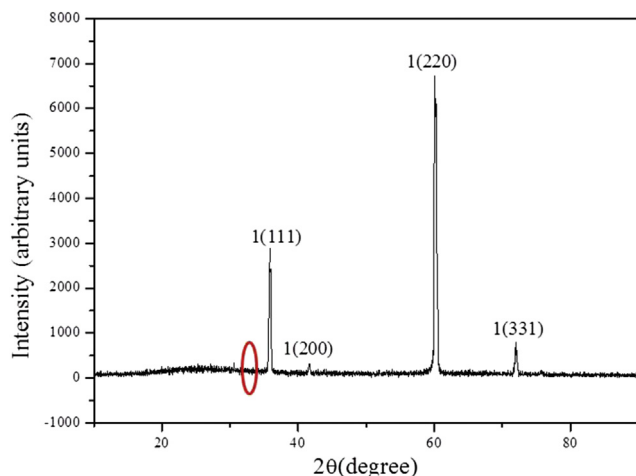


Fig. 2. XRD pattern of the synthesized SiC fibers.

TEM is further carried out to investigate the microstructure of 3C–SiC as shown in Fig. 4. With the help of HRTEM image and SEAD pattern inset in Fig. 4a, the straight SiC fibers have a homogenous crystalline structure with fringes spacing of 2.51 Å, which is characteristic of 3C–SiC. TEM pattern of the bamboo-like is shown in Fig. 4b. It shows that the bamboo joint area is composed of microtwins. The other area has a homogenous crystalline structure with fringes spacing of 2.51 Å. This is in agreement with our recent work [41].

3.2. Characterization of SiC fibers with membrane structure

The pore size of self-assembled SiC fibrous membrane is

investigated by bubble-point method as showed in Fig. 5. It can be seen that the SiC fibrous membrane exhibits the typical membrane character with the smallest pore size, the bubble point pore size (the largest pore size) and mean pore size to be 0.8817 μm, 2.917 μm and 1.603 μm, respectively. Membrane with smaller size can be controlled by adjusting the reaction condition and more work will be carried out.

3.3. High temperature properties

3.3.1. Thermal expansion

Fig. 6 illustrates the linear thermal expansion coefficient of SiC fibers from room temperature to 750 °C and then cooled to room temperature as a cycle at the rate of 10 °C/min in nitrogen atmosphere. According to Eq. (1), the linear thermal expansion coefficient of SiC fibers in the two experimental cycles is calculated to be 4.385×10^{-6} and $4.655 \times 10^{-6}/^{\circ}\text{C}$ respectively, which is close to the theoretical value in the literature, i.e. $4.45 \times 10^{-6}/^{\circ}\text{C}$ [45]. It shows that synthesized SiC fibers have low thermal expansion at high temperature.

3.3.2. Non-isothermal oxidation behavior

Fig. 7 shows the non-isothermal oxidation behavior of SiC fibers from 600 to 1500 °C in dry air. It can be seen that the oxidation reaction starts from about 700 °C and the mass gain rate increases rapidly from 1100 °C until 1500 °C. The microstructure after oxidation (Fig. 7b) indicates that the diameter becomes larger due to crystal growth at high temperature. While the length becomes shorter after oxidation. The main reason is that the difference of thermal expansion coefficient between the oxide product, SiO₂ and SiC fibers. This leads the long fibers to break into short ones. After all, it still remains the fibrous microstructure, indicating the good thermal stability of SiC fibers.

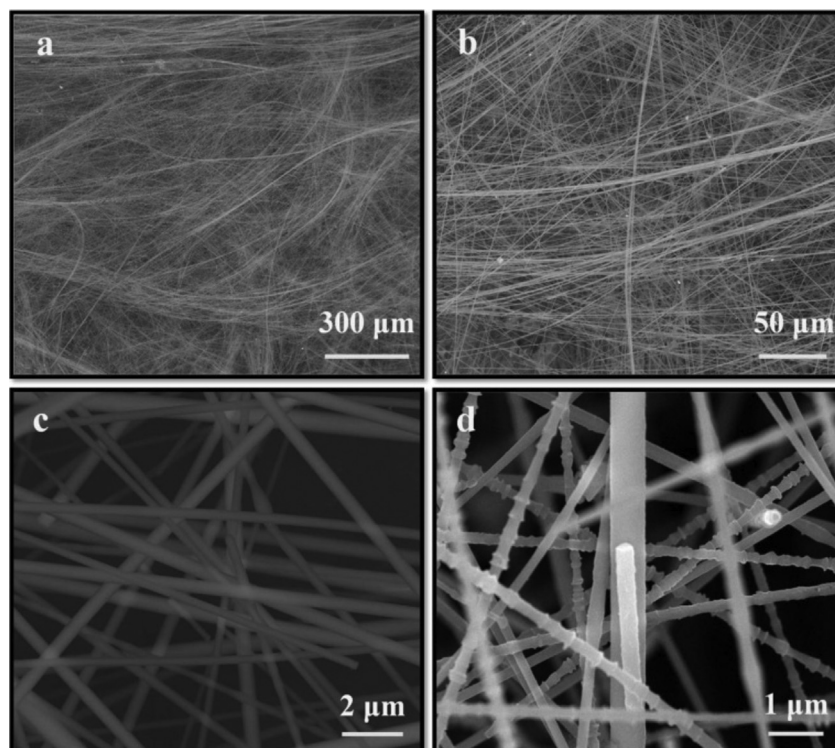


Fig. 3. SEM images of SiC fibers (a, b) low magnification, (c) high magnification of the majority of fibers, (d) high magnification of the minority of fibers.

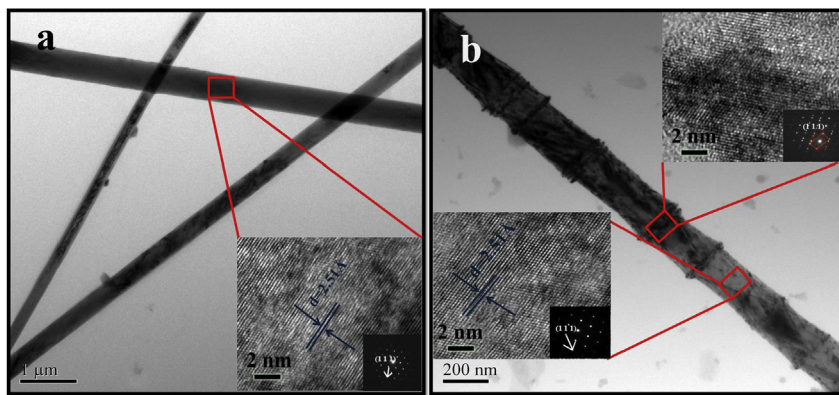


Fig. 4. TEM and HRTEM with corresponding SAED images of SiC fibers (a) the majority of fibers, (b) the minority of fibers.

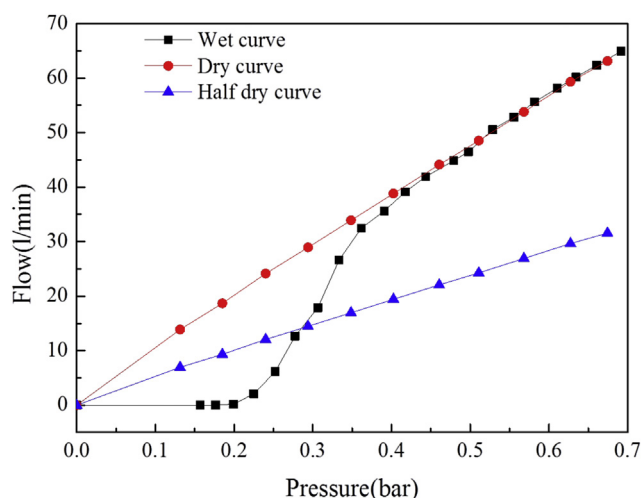


Fig. 5. The pore size of the synthesized SiC fibers with self-standing membrane structure.

3.3.3. Isothermal oxidation behavior

The isothermal oxidation behavior of SiC fibers from 1250 to 1450 °C with 100 °C interval in dry air for 2 h is shown in Fig. 8. It can be seen that the mass gain percent is proportional to temperature, i.e. the total mass change percent gains with temperature increasing. At fixed temperature, the mass gain percent increases quickly initially and then levels off with extended time, indicating

the oxidation reaction is controlled by diffusion. The maximum weight gain percent in this experiment is 28.6% oxidized at 1450 °C. This is far smaller than the theoretical maximum weight gain percent (50%) according to the following reaction:



The microstructure of SiC fibers after isothermal oxidation is also investigated (Fig. 9). It can be seen that the fibrous microstructure remains after oxidation at 1250 °C for 2 h (Fig. 9a) while the diameter becomes larger due to the crystal growth at high temperature. This is similar to that after non-isothermal oxidation as shown in Fig. 7b. At high magnification, some swells appear along the length of the fibers as marked by blue circles (in the web version) in Fig. 9b. EDS analysis (Fig. 9c) shows that the swells are composed of Si and O with the atom ratio of 1:2, indicating they are silica. It has been pointed out that part of the microstructure of SiC fibers contains bamboo-like morphology (Fig. 4b). The bamboo joint area is composed of microtwins, which belongs to a kind of defects and has a priority to be oxidized when exposed to air. With reaction time extending, the oxide layer at the bamboo joint area grows thicker and thus swells are formed. With temperature increasing to 1350 °C, the evolution of whole morphology is more obvious due to the decrease of the reaction energy barrier. As a result, the fibrous microstructure remains (Fig. 9d) while its length becomes relatively shorter as shown in Fig. 9e and f. It should be attributed to the different thermal expansion coefficient between SiO₂ and SiC fibers at the

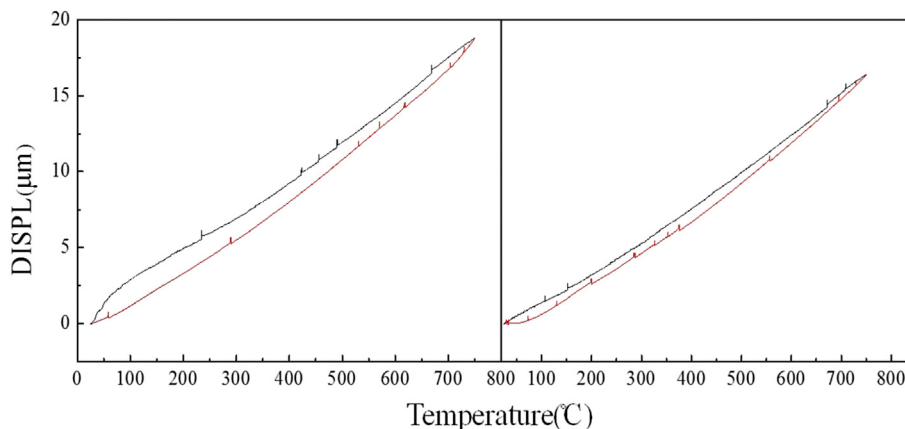


Fig. 6. Relationship between the thermal elongation and temperature of SiC fibers from room temperature to 750 °C at nitrogen atmosphere.

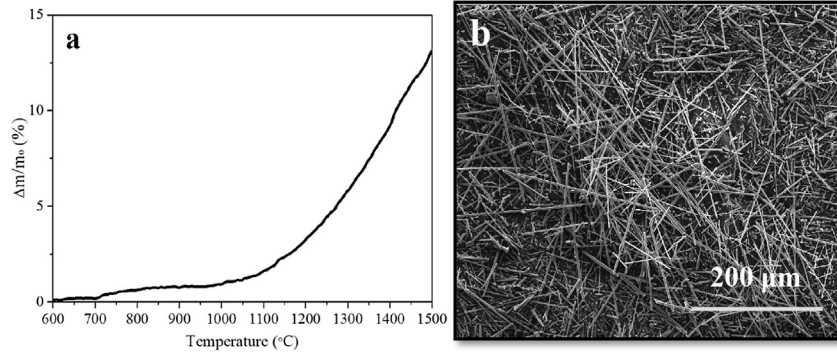


Fig. 7. TG curve (a) and SEM image (b) for SiC fibers after non-isothermal oxidation from 600 to 1500 °C in air.

swell part marked by the circle in Fig. 9e. The phenomenon becomes more obvious at 1450 °C (Fig. 9g, h and i). As shown in Fig. 9h and i, the oxide products sinter together caused by the impurities such as Fe and Na₂O etc. contained in gangue, making porous membrane surface change into dense clusters of SiO₂ crystals (as shown by red circle in Fig. 9h). Due to the formation of the dense SiO₂ layer, it blocks the pathway of oxygen to reach the reaction interface and makes the oxidation proceed very slowly with time prolonging.

In view of the oxidation kinetics of SiC fibers, it belongs to gas–solid reaction. Recently our work group has investigated the oxidation of non-oxide materials and developed a new kinetic model, real physical picture model (RPP model) [46]. In this model, the reacted fraction ξ of oxidation is expressed explicitly as the function of such variables as time t , temperature T , gas partial pressure P_{gas} and sample size etc. Compared with the parabolic rate and linear rate law which are widely adopted to deal with the oxidation of non-oxide materials [47,48], the main difference between the models used in the literature and RPP model is that RPP model is a simpler and physical meaningful explicit analytic model. Importantly, the effect of sample shape on the oxidation behavior can be quantitatively discussed using RPP model [49]. In the following section, the oxidation kinetics of SiC fibers will be discussed using RPP model.

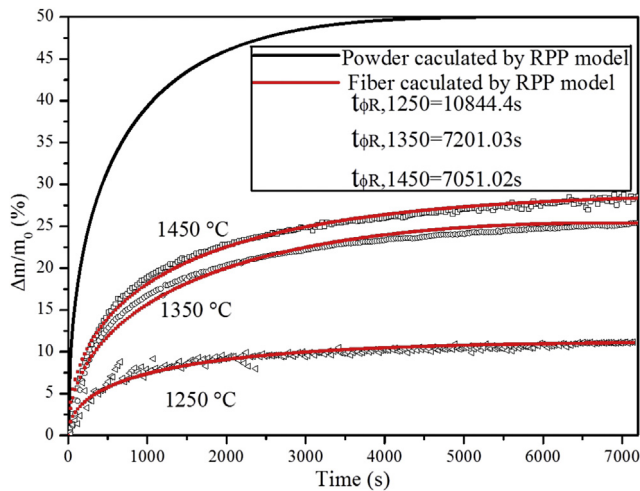


Fig. 8. Comparison of the experimental data and the calculated results by RPP model for isothermal oxidation of SiC fibers (red line at 1250, 1350 and 1450 °C) and SiC powder (black line at 1250 °C) in air for 2 h. (For interpretation of the references to color in this figure legend, the reader is referred to the web version of this article.)

According to RPP model, the oxidation behavior of SiC fibers can be expressed as following:

$$\xi = 1 - \left[1 - \frac{1}{R_0} \sqrt{\frac{2D_0^0 k_0^0 (\sqrt{p_{O_2}} - \sqrt{p_{O_2}^{eq}})}{v_m \exp(\Delta E_d / RT)} t} \right]^2 \times \left[1 - \frac{2}{h_0} \sqrt{\frac{2D_0^0 k_0^0 (\sqrt{p_{O_2}} - \sqrt{p_{O_2}^{eq}})}{v_m \exp(\Delta E_d / RT)} t} \right] \quad (3)$$

where ξ represents the reaction fraction; ΔE_d represents the apparent activation energy (kJ mol⁻¹); $K_0^{O\beta}$ and $D_0^{O\beta}$ are pre-exponential factors; v_m is the density of the sample; R_0 and h_0 is the radius and length of the whole particle, respectively; p_{O_2} and $p_{O_2}^{eq}$ is the partial pressure of oxygen in gas phase and the gas partial pressure in equilibrium with oxide, respectively.

Since the fibers can be taken as a long cylinder with a very small radius, i.e. $h_0 \gg R_0$ therefore Eq. (3) can be simplified to the following approximate form:

$$\xi \approx 1 - \left[1 - \frac{1}{R_0} \sqrt{\frac{2D_0^0 k_0^0 (\sqrt{p_{O_2}} - \sqrt{p_{O_2}^{eq}})}{v_m \exp(\Delta E_d / RT)} t} \right]^2 \quad (4)$$

To simplify the above equation, a parameter $t_{\phi R}$ called characteristic oxidation time is introduced as follows:

$$t_{\phi R} = \frac{1}{\frac{2D_0^0 k_0^0 (\sqrt{p_{O_2}} - \sqrt{p_{O_2}^{eq}})}{v_m R_0^2 \exp(\Delta E_d / RT)}} \quad (5)$$

it can be seen that, the “characteristic oxidation time” $t_{\phi R}$ is the function of such factors as the radius of the cylinder, the oxidation partial pressure, the character of medium where the oxygen pass through as well as the property of reactant and product materials. However, it has no relation with the oxidation time, that is why one can select this parameter to measure the oxidation resistance.

Substituting Eq. (6) into Eq. (5) yields:

$$\xi = 1 - \left[1 - \sqrt{\frac{t}{t_{\phi R}}} \right]^2 \quad (6)$$

Note that the y-axis in the experimental plots (Fig. 8) is mass gain percent $\Delta m/m_0$ instead of the reacted fraction ξ . A transformation is required according to the following equation:

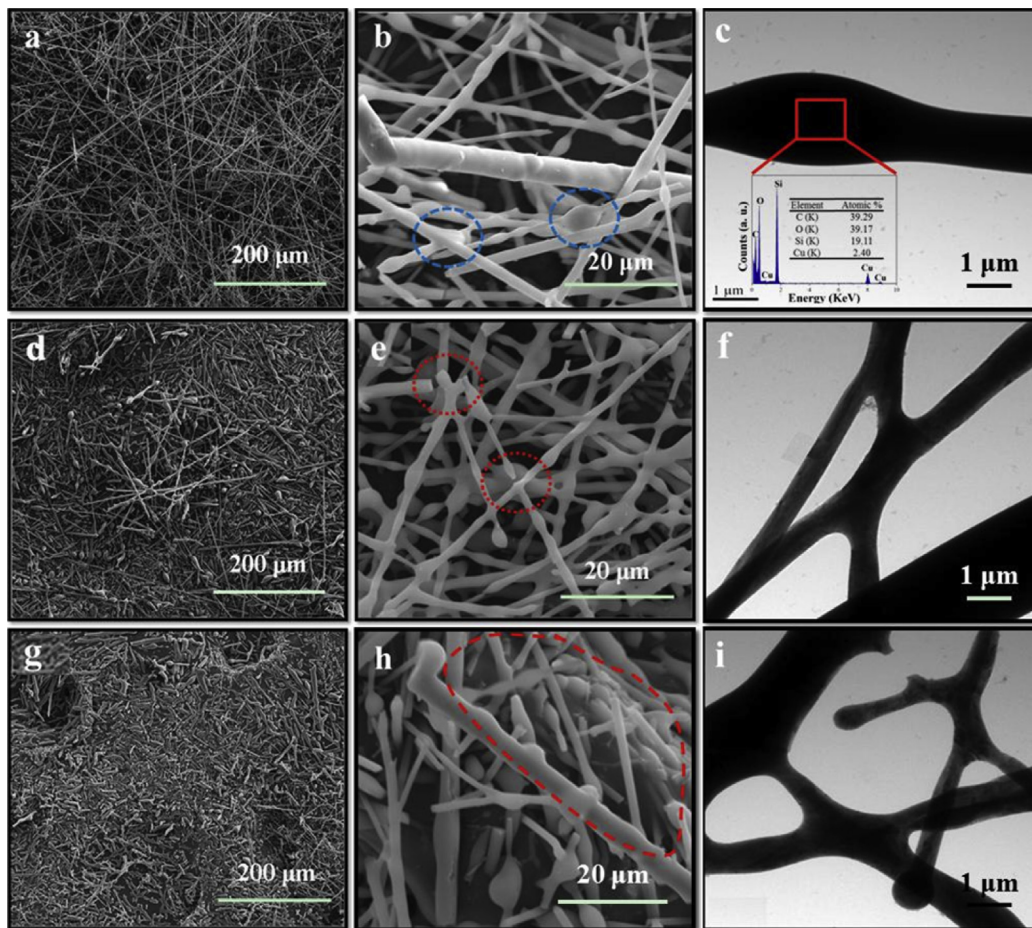


Fig. 9. SEM and TEM images of SiC fibers after oxidation in air for 2 h at different temperature (a, b, c with EDS result) 1250 °C, (d, e, f) 1350 °C, (g, h, i) 1450 °C.

$$\xi = \frac{\Delta m/m_0}{\Delta m_{\max}/m_0} \quad (7)$$

where Δm_{\max} is the corresponding maximum increment after oxidation up to 2 h at different temperature.

By regression method, the characteristic oxidation time ($t_{\phi R}$) under the three temperature is 10844.4 s, 7201.03 s and 7051.02 s respectively, indicating the oxidation resistance of the fibers decreases with increasing temperature. The curves obtained from the above equations are also shown in Fig. 8 as red line, which fits the experimental data fairly well, validating the reasonability of RPP model. In addition, the mass change percent of SiC powder with the average particle size of 300 nm at 1250 °C is predicted to be 50% using RPP model [49] as shown as black line in Fig. 8. By comparison, the mass change percent of SiC fibers with the similar diameter at 1250 °C is much lower (11.2%), further verifying the better oxidation resistance of SiC fibers.

4. Conclusions

High purity 3C–SiC fibers with the diameter in the range of 100–500 nm and length up to several millimeters are synthesized using one-step and economical carbon thermal reduction method. The synthesized SiC fiber is self-assembled into membrane with the average pore size of 1.603 μm. In view of the high temperature properties, SiC fibers exhibit low thermal expansion coefficient and better oxidation resistance up to 1250 °C. RPP model is adopted to

deal with the oxidation kinetics and gets good agreement with the experimental data by introducing the parameter of the characteristic oxidation time $t_{\phi R}$. Combining these properties, SiC fibers with a self-standing membrane structure can be a promising candidate used at high temperature.

Acknowledgments

The authors express their appreciation to National Nature Science Foundation of China of No. 51104012, the National Science-technology Support Plan Projects of No. 2013BAF09B01 and the Central Universities of No. FRF-SD-13-006A for financial support.

References

- [1] Q. Wei, D. Shao, B. Deng, Q. Xu, J. Coat. Technol. Res. 7 (2010) 99–103.
- [2] Y.H. Liu, R.J. Ji, Q.Y. Li, L.L. Yu, X.P. Li, J. Alloys Compd. 472 (2009) 406–410.
- [3] F.Y. Yang, X.H. Zhang, J.C. Han, S.Y. Du, J. Alloys Compd. 472 (2009) 395–399.
- [4] D.B. Marshall, A.G. Evans, J. Am. Ceram. Soc. 68 (1985) 225–231.
- [5] S. Kumar, K.M. Reddy, A. Kumar, G.R. Devi, Aerosol Sci. Technol. 26 (2013) 185–191.
- [6] T.E. Kim, J.C. Bae, K.Y. Cho, Y.G. Shul, C.Y. Kim, J. Nanosci. Nanotechnol. 13 (2013) 3307–3312.
- [7] M. Singh, T. Matsunaga, H.T. Lin, R. Asthana, T. Ishikawa, Mater. Sci. Eng. A 557 (2012) 69–76.
- [8] F. Wan, F. Luo, Y. Zhou, W. Zhou, D. Zhu, Surf. Coat. Technol. 264 (2015) 9–16.
- [9] H. Liu, H. Cheng, J. Wang, G. Tang, J. Alloys Compd. 491 (2010) 248–251.
- [10] A.S. Prosviryakov, J. Alloys Compd. 632 (2015) 707–710.
- [11] R.V. Krishnarao, J. Subrahmanyam, S. Subbarao, Bull. Mater. Sci. 24 (2001) 273–279.
- [12] N.L. Shi, K. Luo, Y.P. Zu, Y.D. Duan, J. Mater. Sci. Technol. 16 (2000) 637–638.
- [13] W.J. Lackey, J.A. Hanigofsky, G.B. Freeman, R.D. Hardin, A. Prasad, J. Am. Ceram.

- Soc. 78 (1995) 1564–1570.
- [14] N. Chaabane, M.L. Flem, M. Tanguy, S. Urvoy, C. Sandt, P. Dumas, Y. Serruys, *J. Nucl. Mater.* 439 (2013) 123–130.
- [15] L. Xiong, Y. Xu, Y. Li, X. Xia, *J. Mater. Sci.* 43 (2008) 4849–4855.
- [16] K. Suzuya, M. Furusaka, N. Watanabe, M. Osawa, K. Okamura, K. Shibata, K. Suzuki, *J. Mater. Sci.* 11 (1996) 1169–1178.
- [17] H. Hou, F. Gao, G. Wei, M. Wang, J. Zheng, B. Tang, W. Yang, *Cryst. Growth Des.* 12 (2012) 536–539.
- [18] Z.Y. Chu, C.X. Feng, Y.C. Song, X.D. Li, J.Y. Xiao, Y.D. Wang, *J. Inorg. Mater.* 17 (2002) 193–201.
- [19] B.G. Penn, F.E. Ledbetter, J.M. Clemons, J.G. Daniels, *J. Appl. Polym. Sci.* 27 (1982) 3751–3761.
- [20] M. Takeda, A. Urano, J.I. Sakamoto, Y. Imai, *J. Am. Ceram. Soc.* 83 (2000) 1171–1176.
- [21] Z.Y. Chu, Y.C. Song, C.X. Feng, Y.S. Xu, Y.B. Fu, *J. Mater. Sci. Lett.* 20 (2001) 585–587.
- [22] D.F. Zhao, H.Z. Wang, X.D. Li, *J. Inorg. Mater.* 24 (2009) 1097–1104.
- [23] S. Chen, P. Ying, L. Wang, G. Wei, F. Gao, J. Zheng, T. Wu, *NPG Asia Mater* 7 (2015) e157.
- [24] L. Wang, G. Wei, F. Gao, C. Li, W. Yang, *Nanoscale* 7 (2015) 7585–7592.
- [25] L. Wang, C. Li, Y. Yang, S. Chen, F. Gao, G. Wei, W. Yang, *ACS Appl. Mater. Inter.* 7 (2014) 526–533.
- [26] S. Chen, P. Ying, L. Wang, G. Wei, W. Yang, *Appl. Phys. Lett.* 105 (2014) 133106.
- [27] Y. Yang, H. Yang, G. Wei, L. Wang, M. Shang, Z. Yang, W. Yang, *J. Mater. Chem. C* 2 (2014) 4515–4520.
- [28] S. Chen, Y. Ying, L. Wang, F. Gao, G. Wei, J. Zheng, W. Yang, *RSC Adv.* 4 (2014) 8376–8382.
- [29] S. Chen, P. Ying, L. Wang, G. Wei, J. Zheng, F. Gao, W. Yang, *J. Mater. Chem. C* 1 (2013) 4779–4784.
- [30] Z. He, L. Wang, F. Gao, G. Wei, J. Zheng, X. Cheng, W. Yang, *CrystEngComm* 15 (2013) 2354–2358.
- [31] I. Hasegawa, T. Nakamura, S. Motojima, M. Kajiwara, *J. Sol-gel Sci. Technol.* 8 (1997) 577–579.
- [32] Z.H. Pan, Z.H. Huang, W.J. Li, Y.G. Liu, M.H. Fang, *Key Eng. Mater.* 512 (2012) 7–10.
- [33] A.R. Bunsell, A. Piant, *J. Mater. Sci.* 41 (2006) 823–839.
- [34] Y.J. Hao, G.Q. Jin, X.D. Han, X.Y. Guo, *Mater. Lett.* 60 (2006) 1334–1337.
- [35] S. Dhage, H.C. Lee, M.S. Hassan, M.S. Akhtar, C.Y. Kim, J.M. Sohn, O.B. Yang, *Mater. Lett.* 63 (2009) 174–176.
- [36] G.W. Meng, Z. Cui, L.D. Zhang, F. Phillipp, *J. Cryst. Growth* 209 (2000) 801–806.
- [37] Y.J. Lee, *Diam. Relat. Mater.* 13 (2004) 383–388.
- [38] Y. Shin, C. Wang, G. Exarhos, *Adv. Mater.* 17 (2005) 73–77.
- [39] W. Wang, Z. Jin, T. Xue, G. Yang, G. Qiao, *J. Mater. Sci.* 42 (2007) 6439–6445.
- [40] H.J. Hwang, K.J. Lee, Y.T. An, B.H. Choi, W.S. Seo, *Mater. Chem. Phys.* 134 (2012) 13–15.
- [41] J.H. Chen, W.N. Liu, T. Yang, B. Li, J.D. Su, X.M. Hou, K.C. Chou, *Cryst. Growth Des.* 14 (2014) 4624–4630.
- [42] E. Jakobs, W.J. Koros, *J. Membr. Sci.* 124 (1997) 149–159.
- [43] M. Kato, H. Konishi, M. Hirata, *J. Chem. Eng. Data* 15 (1970) 435–439.
- [44] H. Tateyama, N. Sutoh, N. Murukawa, *J. Ceram. Soc. Jpn.* 386 (1988) 1003–1011.
- [45] Z. Li, R.C. Bradt, *J. Mater. Sci.* 21 (1986) 4366–4368.
- [46] K.C. Chou, X.M. Hou, *J. Am. Ceram. Soc.* 92 (2009) 585–594.
- [47] L.U. Ogbuji, M. Singh, *J. Mater. Res.* 10 (1995) 3232–3240.
- [48] S.C. Singhal, *J. Mater. Sci.* 11 (1976) 1246–1253.
- [49] X.M. Hou, Z.Y. Yu, Z.Y. Chen, B.J. Zhao, K.C. Chou, *Dalton. T.* 41 (2012) 7127–7133.